Superlattices and Microstructures, Vol. 25, No. 5/6, 1999
Article No. spmi.1999.0750
Available online at http://www.idealibrary.com on IDEAL

Nano-ploughed Josephson junctions as on-chip radiation sources

B. IRMER, F. SIMMEL, R. H. BLICK, H. LORENZ, J. P. KOTTHAUS
Center for NanoScience and Sektion Physik, Ludwig-Maximilians-Universität, 80539 München, Germany

M. BICHLER, W. WEGSCHEIDER
Walter Schottky Institut, TU München, Am Coulombwall, 85748 Garching, Germany

(Received 24 March 1999)

A new technique is presented which enables the fabrication of highly transparent Josephson junctions in combination with mesoscopic devices. We utilize a modified AFM tip to plough grooves into superconducting material, thus defining a weak link. This weak link is made within the superconducting split-gates, which are used to electrostatically form a conventional quantum dot and serves as a source of millimeter wave radiation around 100 GHz. We show the characteristics of typical junctions built and discuss their high-frequency properties. We find that the millimeter wave emission of the weak link leads to a bolometric effect in the case of quantum point contact spectroscopy.

Key words: mesoscopics, quantum dots, Josephson junctions.

1. Introduction

Direct mechanical structuring does not seem to be the obvious method to build mesoscopic devices. Nevertheless, we applied the fairly ancient technique of ploughing[†] with modified AFM tips to build Josephson junctions (JJs) [1] in conjunction with standard mesoscopic systems, e.g. quantum point contacts [2], single and double quantum dots [3]. The main advantages of our approach are the ease of integration of the different techniques and the flexibility to build spectroscopic tools in the quantum limit. While conventional spectroscopy on mesoscopic structures relies on bulky external frequency sources, our aim is to place the millimeter wave sources at a nanometer distance from the device under test. This not only allows the generation of high-intensity electromagnetic fields exactly at the nanostructure, minimizing effects by external heating, but also spectroscopy on quantum structures and the investigation of coherent electron tunneling phenomena directly in the frequency domain.

In the first part of this work we focus on the general properties of JJs, on the fabrication and also present characteristic measurements of these millimeter wave sources. Moreover, we discuss the suitability of the ploughing technique to mechanically form coupled JJs. Then we present first measurements on a quantum point contact coupled to a single junction's radiation and finally we discuss the possibility of applying the sources for spectroscopy on quantum dot devices.

[†]The Sumerians not only invented the wheel around 3700 BC but also the plough around 3200 BC, which can both be regarded as major milestones in the history of human civilization.

0749–6036/99/050785 + 11 $30.00/0

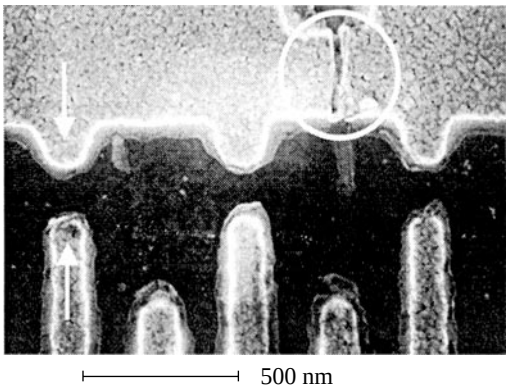

Fig. 1. SEM micrograph of a double quantum dot with an embedded nanoploughed weak-link. The white arrows indicate the gates swept for the QPC measurement shown in Fig. 9. The circle indicates the position of the JJ.

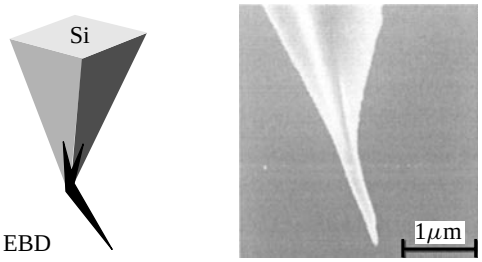

Fig. 2. Left: a schematic sketch of the nanoploughs used. Note the side coverage to ensure a stable and robust interface between the basic silicon tip and the EBD plough. Right: electron microscope image of a typical tip.

2. Fabrication

2.1. Why plough the Josephson junctions?

In the history of prediction and discovery of the Josephson effect [4] a major role was played by tunnel junctions, where the two superconducting reservoirs are weakly connected by a thin insulating barrier. However, the coupling between the reservoirs can be realized by any means as long as it is 'weak', i.e. the order parameter is suppressed locally but the reservoirs do not become completely independent from each other. In very different types of junctions the Josephson effect has been observed, e.g. point contacts [5], proximity effect bridges [6], superconductor/normal/superconductor systems and micro-patterned thin film systems (Dayem bridge [7] and variable thickness bridge [8]) to name only the most prominent.

The radiation generated by the ac Josephson current should couple into the environment with a nonvanishing efficiency and the fabrication of the junction has to be fully compatible with the preparation of the quantum dot system. As an example, Fig. 1 shows an electron microscope image of a GaAs/AlGaAs heterostructure with aluminium gates on top of it, which electrostatically define two quantum dots separated by tunable tunnel barriers. The JJ has to be placed as close as possible to the quantum dots (precision in alignment) and its integration has to be fully compatible with the quantum dot system (best made out of the same thin film). This adds serious technological complications.

In the following we will discuss their use for this purpose from a technological point of view as well as from their ac Josephson behavior: tunneling JJs require high-quality and very thin (thickness $d \approx 10$ to 20) oxide barriers. This is commonly achieved by thermal oxidation of the first electrode, on top of which the second

metallic electrode is placed. This sets very high goals for the patterning and alignment and minimizes the yield in this process when combined with the quantum dot definition, which is nontrivial itself. Furthermore, tunnel junctions suffer from comparably low critical Josephson current densities $j_c \approx 10^2$ A cm^{-2} [9], which are limited by the tunnel resistance $R_n \approx 1$ kΩ. The efficiency with which radiation can decouple depends not only on the material's specific permittivity ϵ_r but also on the junction's dimension: the wave propagates with the Swihart velocity $\tilde{c} = c_0/\sqrt{\epsilon_r(1 + 2\lambda_L/L)}$ [10], wherein λ_L is the London penetration depth and L is the length of the barrier. The impedance of the JJ is then $Z_J = c_0/\tilde{c} \cdot (L/\epsilon_r W) \cdot Z_0$ [10] where the free space impedance $Z_0 = 377\ \Omega$ and W is the width of the barrier. In oxide junctions the length L is defined by the thickness of the tunneling barrier, whereby $L \ll \lambda_L$. This results in $\tilde{c} \ll c_0$ and the coupling to the environment will be very inefficient, e.g. for $L \approx 10$ the impedance becomes $Z_J \approx 10^{-4} Z_0$. Another important aspect is the large intrinsic capacitance C of the junction, which effectively shunts the tunnel conductance at higher frequencies [11].

Microbridges, however, are in general expected to show nearly ideal Josephson behavior if its dimensions L_{eff} are sufficiently small relative to the coherence length ξ [12]. Their main advantage is the lower resistance $R_n \approx 0.1\ \Omega$, and hence the higher critical current densities j_c of typically 10^6 A cm^{-2}. This is expected to result in a dramatically enhanced microwave emission. Furthermore, the length L of the bridge can be made comparable to λ_L, which results in a better impedance matching between the junction and the environment, e.g. for $L = 100$ nm, Z_J becomes $1/3 Z_0$.

Common techniques for weak link fabrication are cutting thin films with razor blades or diamond scratchers [13–15]. Although bridges down to some 0.1 μm have been made, they cannot be positioned into predefined gate structures with the same precision. Nevertheless, nanometer precision is standard for scanning probe microscopes, both in imaging and patterning [16]. By giving the tip the functionality of a tool, e.g. a plough, one can accurately position the tool within the gate structure of the quantum dot device, remove thin film material in a well-defined way, and leave behind trenches which then define microbridges of constant or variable thicknesses. The advantages of applying a nanoplough for lithography are obviously the precision of alignment, the nondamaging definition process compared to electron or ion beam lithography, and the absence of additional processing steps, such as etching the substrate.

We define our devices in Al thin films with a thickness around 100 nm, which are thermally evaporated[‡] onto semi-insulating GaAs substrates for the I–V characteristics and GaAs/AlGaAs heterostructures for the quantum point contact measurements. Wire and gate structures are predefined with optical and electron beam lithography.

2.2. Tools used: nanoploughs

A crucial point for nanoploughing is the appropriate plough: common scanning probe microscope tips are either robust but too blunt to form small trenches (Si_3N_4 or hard coated tips) or too brittle for this purpose (single crystal Si). We employ *electron beam deposition* (EBD) to grow material onto the end of common Si tips by focusing the beam of a scanning electron microscope. The highly energetic electrons interact with additionally introduced organic gases and form an organic compound, known as high dense carbon [16]. This material shows a hardness comparable to that of diamond [17] in combination with being nonbrittle [18]. Special care has to be taken to ensure a robust interface between the EBD tip and the silicon pyramid. This is done by first growing a tripod onto the sides of the Si tip before growing the plough itself. This gives a high stability to withstand shear forces. For the nanoplough, 500 nm long and 50 nm wide needle-like tips are grown under a nonzero angle with respect to the axis of the pyramidal Si tip. When dragged through the

[‡]In order to achieve reasonable superconducting properties, we use high evaporation rates $\approx$100 and low background pressure, typically at $p \leq 10^{-7}$ mbar. The critical temperature T_c is typically slightly above 1 K for thin films.

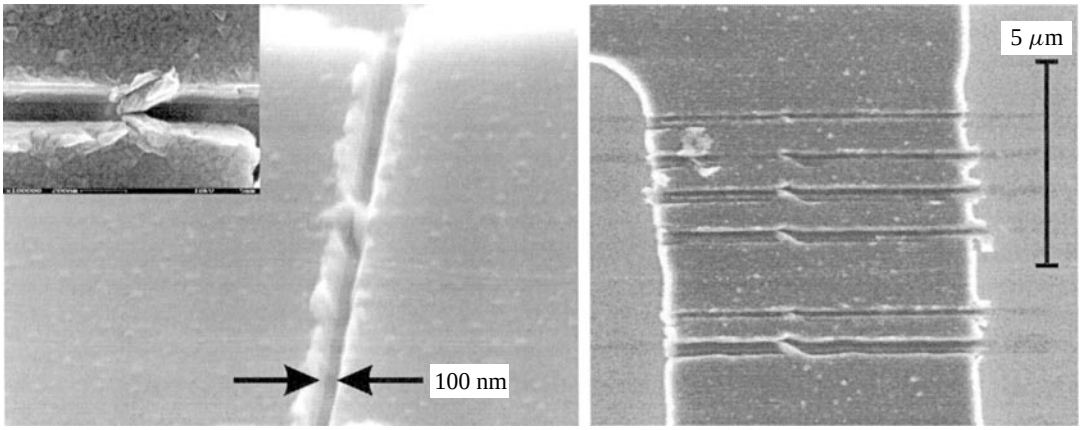

Fig. 3. Nano-ploughed lines in an Al film. Left: a typical Dayem-style microbridge with dimensions $L \times W = 100\ \text{nm} \times 100\ \text{nm}$. Right: the loading force is increased from top to bottom, defining variable thickness bridges and bridges of increasing length L. The junction width W is easily adjusted by a horizontal displacement W, where the plough is withdrawn from the film.

material this angle causes an additional vertical force component which ensures that the plough is pushed downwards, cutting its way through the material.

2.3. Ploughing of superconducting thin films

Imaging and positioning is performed in standard AFM mode.[§] In the ploughing mode, the tip is displaced nominally by Δz towards the surface, resulting in a loading force $F_\perp \approx k \cdot \Delta z$. Cantilevers with high force constants $k \approx 40$–$100\ \text{N m}^{-1}$ are used. The vertical displacement ranges from $\Delta z \approx 0.1\ \mu\text{m}$ to several micrometers, offering a wide range of loading forces. These can be sufficient to completely remove the metal layer or to form a trench with a residual base thickness. To define a microbridge of width W, the tip is withdrawn from the surface, displaced by a length W and driven into the metal layer again. The length L of the Josephson contact is defined by the width of the trench, which again is given by the tip diameter. To date we were able to cut 300 nm thick Al films with a minimum line width of 50 nm, yielding an aspect ratio of 1 : 6. In Fig. 3 several trenches under various ploughing conditions are shown.

For all lines the same tip has been used and the ploughing speed was $100\ \text{nm s}^{-1}$ throughout. The vertical displacement Δz is increased from 0.5 μm for the top line to 2.5 μm at the baseline. For the indentation pressure involved we can estimate 1 to 100 GPa, whereas the hardness of evaporated Al is about 0.5 GPa [19]. The Al film is cut in a very controlled way, the removed material is placed on both sides of the trench. In this way multiple JJ arrays can be made with a spacing close to L. Weak scratches in the GaAs substrate can be seen, thus ensuring that all the material has been removed from the film.

With appropriate parameters, either Dayem-bridge-type weak links with constant film thickness, or variable thickness bridges or even a combination of both can be fabricated. As an example, a Dayem bridge with dimensions $W \times L = (100 \times 100)\ \text{nm}^2$ is shown in the left part of Fig. 3.

[§] Imaging is done in dynamic AFM, commonly called Tapping Mode. This ensures a nondestructive imaging even when cantilevers with high force constants are used.

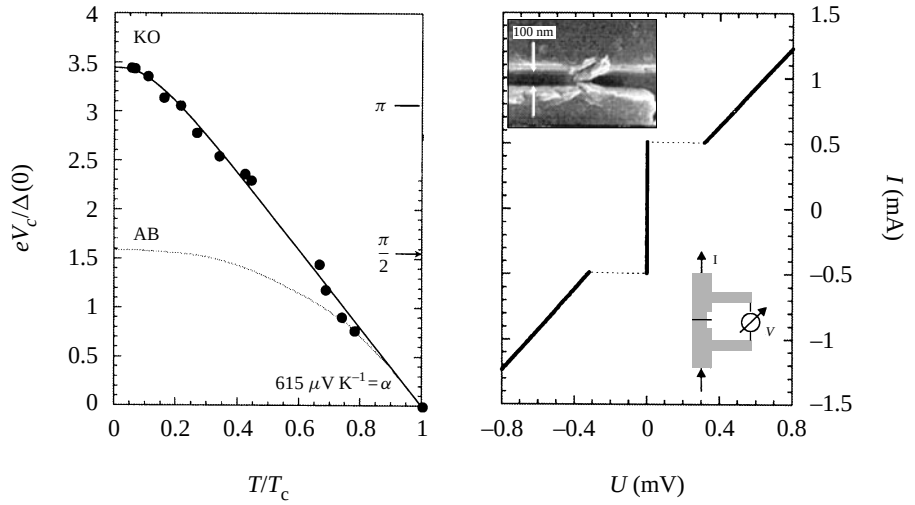

Fig. 4. Left: from the temperature dependence, our junction (black dots) is interpreted as a clean weak link with $L \ll l, \xi$ (Kulik and Omelyanchuk: KO). KO theory predicts a critical current of π for $T/T_c = 0$. The universal slope $\alpha = \partial(R_N \cdot I_c)/\partial T$ for $T \to T_c$ implies $\alpha = 615\ \mu\text{V K}^{-1}$, in good agreement with the theoretical value $\alpha = 635\ \mu\text{V K}^{-1}$. This device shows a critical temperature $T_c = 950$ mK. Right: characteristic I–V trace of a Dayem-bridge-style junction at $T = 35$ mK.

3. Characterization of Josephson junctions

3.1. High transparency

All transport measurements are conducted in a standard current feed four-probe setup in a dilution refrigerator at 35 mK. First we look at the temperature dependence of the critical current density (Fig. 4), which is estimated to be $j_c(T \to 0) = I_c/L{\cdot}d = 5.1{\times}10^6$ A cm^{-2}, where d is the thickness of the film. From the temperature dependence of the critical voltage $V_c = I_c \cdot R_n$ (Fig. 3), we reproduce the universal material-independent slope $\alpha = \partial(R_N \cdot I_c)/\partial T = 2\pi k_B/7\zeta(3)e$ for $T \to T_c$. This also identifies the conduction mechanism inside the junction: the Kulik–Omelyanchuk theory (KO: straight line) [20] for the case of a clean weak link, i.e. $\xi, l \gg L_{eff}$, where l is the mean free path of electrons and ξ the coherence length, fits very well to our data. A tunnel junction in comparison gives much lower critical currents (Ambegaokar–Baratoff: AB) [21].

From its critical temperature we calculate the BCS gap $\Delta_{Al}(T \to 0) = 3.37/2 \cdot k_B T_c = 138\ \mu$eV [22]. The associated clean limit coherence length $\xi_{Al} = 0.18 \cdot \hbar v_F/(k_B T_c)$ is then $\xi_{Al} = 2.9\ \mu$m [23], using the bulk Fermi velocity of $v_F = 2.03 \times 10^6$ m s^{-1}. This should be compared to the effective length L_{eff} of the Josephson constriction, which is somewhat larger than the 100 nm geometric length, but still an order of magnitude smaller than ξ, which makes our junction extremely transparent [9, 24].

3.2. Dayem bridge

Here we only want to describe the main features in the current–voltage characteristics for the two types of microbridges and especially their differences. A detailed description of the observed phenomena is e.g. given in [25].

In Fig. 5 a set of characteristic I–V traces of a single Al junction is shown, where the external magnetic field is increased from zero to 10 mT. The dc Josephson current can be clearly seen. For currents larger than the critical current I_c, a finite voltage drops across the junction, defined by its normal resistance $R_n = 0.57\ \Omega$.

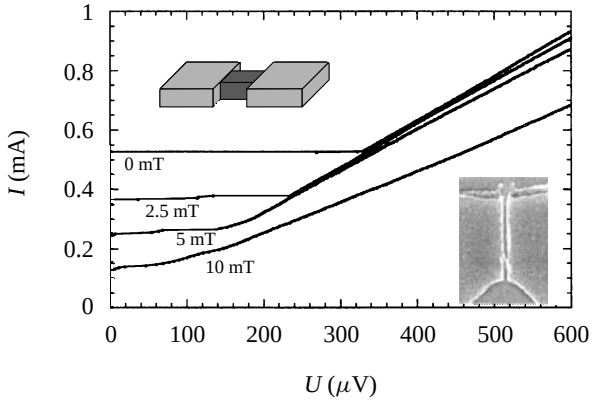

Fig. 5. I–V characteristics of a Dayem-bridge-style Josephson junction under various magnetic fields perpendicular to the film. The critical field B_c is 18 mT. The insets show a schematic view and a micrograph of the actual device.

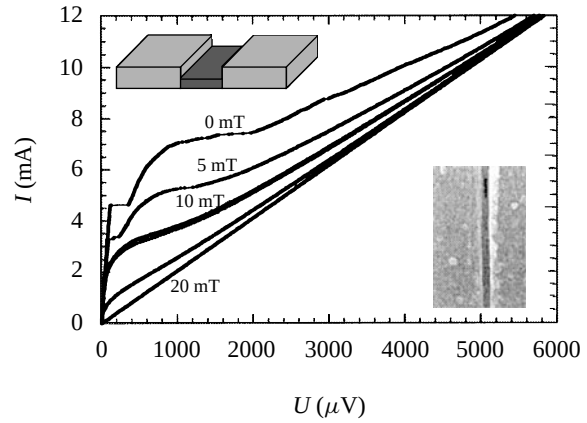

Fig. 6. I–V characteristics of a variable thickness bridge under various magnetic fields. The critical field B_c is 20 mT. The insets show a schematic view and a micrograph of the actual device. Note that the current and voltage axis are enlarged by a factor of 10 in comparison to Fig. 5.

The excess current is close to zero. The I–V characteristics are not hysteretic and single valued. This agrees well with the theoretical description for a nontunneling, Dayem-bridge-like superconducting weak link described by Likharev [9]. For increasing magnetic fields the Josephson current is reduced to zero, i.e. normal conductivity, at $B_c = 18$ mT.

3.3. Variable thickness bridge (VTB)

For the VTBs a very distinct behavior is observed: starting from $V = 0$, a supercurrent accompanied by a finite voltage is found up to about 115 μV, characterized by a differential resistance $R_d = 24.7\ \text{m}\Omega \ll R_n = 0.48\ \Omega$. The I–V characteristics progress, after a small jump in voltage, into a curve with higher resistance. This section shows a significant fine structure. At even larger voltages, the I–V curve bends towards the normal current carrying state defined by R_n, probably due to heating. At this point, the extrapolated characteristics cut exactly through $I = V = 0$. This behavior is very similar to that observed by Klapwijk *et al.* [26], where it is interpreted as a consequence of a phase slip process. A flux flow hypothesis is inapplicable

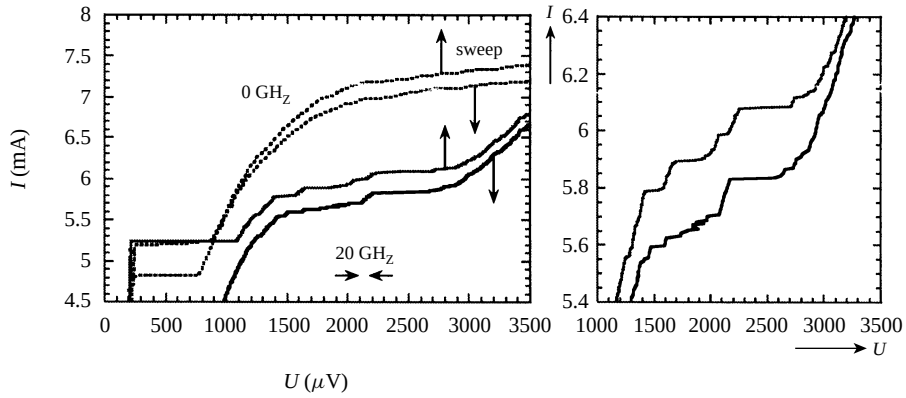

Fig. 7. Left: I–V characteristics of an Al variable thickness microbridge without (0 GHz) and under external microwave radiation of $f = 20$ GHz. Right: detailed view on the steps appearing.

because the sample size is too small to allow vortex penetration [25]. The fine structure can be related to self-resonant modes, where the electromagnetic field associated with the ac current interacts with the external environment and the junction cavity.

3.4. HF response

In order to verify the ac Josephson effect and the microwave response of the nanoploughed bridges, radiation of $f = 20$ GHz from an external source is radiated onto the microbridge. No on-chip antenna or special cavity were used. Clearly the junction does interact with the electromagnetic field and changes its I–V characteristics significantly. The peculiar step-like shape of it can be understood as a superposition of externally induced Shapiro steps and self-resonant modes of the intrinsic Josephson radiation [27].

4. Josephson junction coupled to a quantum point contact

4.1. Bolometric response of a quantum point contact to Josephson radiation

The nanoploughed Josephson junctions can easily be combined with mesoscopic semiconductor structures such as quantum point contacts or quantum dots (Fig. 1). One of the gates is equipped with four terminals to ensure full control of the JJ. The junction itself is defined by nanoploughing at the desired position (as described in Section 2). The two-dimensional electron gas (2DEG) of the GaAs/AlGaAs heterostructure we use is located 50 nm below the surface. It has a sheet density of $n_S = 1.6 \times 10^{11}$ cm^{-2} and a low-temperature mobility of $\mu = 8 \times 10^5$ cm^2 V^{-1} s^{-1}.

As a first demonstration of the influence of the microwave radiation emitted by the weak link on a mesoscopic structure in the 2DEG, we report on the bolometric change in the quantized conductance steps of a quantum point contact (QPC) [2]. Microwave radiation causes heating of the electron reservoirs separated by the QPC which leads to a bolometric photo-conductance signal. The current through a QPC can be written as

$$I = \frac{2e}{h} \int_0^\infty t(E)[\, f(E - \mu_S;\, T_S) - \, f(E - \mu_D;\, T_D)]dE,$$

where $t(E)$ is given by $t(E) = \sum_n \theta(E - E_n)$ with E_n being the nth subband energy of the QPC, and μ_S, T_S and μ_D, T_D the chemical potentials and the local temperatures of the source and drain, respectively [28]. The

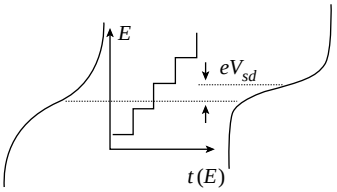

Fig. 8. Different local temperatures of source and drain are the origin of the bolometric response of a QPC to microwave irradiation.

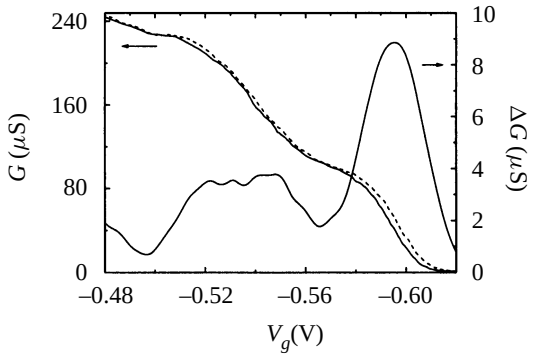

Fig. 9. Measurement of the bolometric response of a QPC to Josephson radiation emitted by the nanoploughed weak link. The step-like curves show the conductance through the QPC without (solid line) and with radiation (dotted line). Substracting the signals with and without radiation, we obtain the bolometric signal displayed to the right axis.

chemical potentials differ by the bias voltage V_{sd} (cf. Fig. 8). The difference between the Fermi distributions of the electrons on either side leads to an enhancement of the current in the regions between the quantized conductance steps [28].

In the experiment one of the quantum point contacts of the quantum dot structure in Fig. 1 was defined in the 2DEG via a field-effect by applying negative voltages V_g to the gates indicated. Across the QPC a bias voltage of $V_{sd} = 300\ \mu$V was applied. The differential conductance of the QPC was measured at a temperature of 35 mK using standard lock-in techniques. The weak link was tuned into the ac Josephson regime with a dc voltage of $V_{JJ} = 500\ \mu$V at zero magnetic field. The measured conductances and the difference signal (photo-conductance) are displayed in Fig. 9. Switching on the weak link clearly results in an enhancement of the conductance in the regions between the conductance plateaus as expected from theory. This demonstrates the feasibility of combining a weak link as an on-chip microwave source with a mesoscopic structure.

5. Applications in photon-assisted mesoscopic transport

Apart from bolometric signals, the phenomena one seeks to observe in the transport properties of mesoscopic structures under the influence of microwave radiation are photon-assisted tunneling and Rabi oscillations. In the tunneling regime, absorption or emission of a photon by a tunneling electron can enable tunneling processes at energies $\pm n\hbar\omega$ normally forbidden by energy conservation [29, 30]. These photon-assisted processes can significantly alter the transport properties of quantum dots in the Coulomb blockade regime. Quantum dots are small electronic islands isolated from the 2DEG by tunneling barriers [3]. In the Coulomb blockade regime $k_BT \ll e^2/C$, where C is the total capacitance of the quantum dot. We find for typical devices, $T \approx 100$ mK and $C \approx 100$ aF. In this regime, transport through the quantum dot is normally

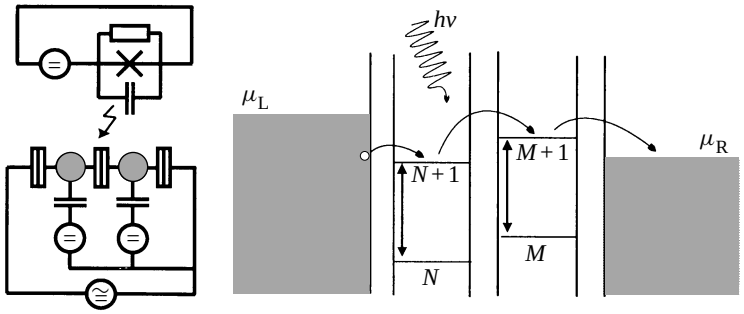

Fig. 10. Left: schematic representation of the double quantum dot with weak link. Right: electron pumping through a double quantum dot under the influence of microwave radiation. Transport through the system is made possible by absorption of photons.

blocked due to the large charging energy for a single electron. However, at certain gate voltages the energy of the dot with N electrons is degenerate with the energy of the dot occupied by $(N + 1)$ electrons. Then, the charge on the dot is allowed to fluctuate resulting in a sharp conductance peak due to tunneling of single electrons onto and off the dot. Photon-assisted tunneling under microwave irradiation leads to the occurence of photon sidebands of these conductance peaks [31–33].

Transport through a double quantum dot system is only possible if, in addition to the requirements for a single quantum dot, an occupied electronic state in one dot is aligned with an accessible state in the other dot. The resulting conductance peaks are even less broadened than in the single quantum dot case, as the thermal broadening induced by the reservoirs is circumvented by this inter-dot resonance criterion. Due to the diminished broadening of the conductance peaks photon sidebands can be observed more clearly and at frequencies below the limit of thermal broadening (usually down to 1 GHz). By appropriately tuning the bias and gate voltages a variety of transport scenarios can be realized [34]. One prominent example is the single electron pump [35]. In a double quantum dot with weak inter-dot coupling, i.e. a large tunneling barrier and a small capacitance between the two dots, electrons can be sequentially pumped through the system under the influence of microwave irradiation as depicted in Fig. 10. If, in contrast, the two quantum dots are strongly coupled, an artificial molecule will be formed. Analogous to molecular physics, the energy levels of the double quantum dot are then tunnel split into bonding and anti-bonding states. Irradiation with microwaves at a frequency corresponding to the tunnel splitting leads to Rabi oscillations within the artificial molecule [36].

Observation of such photon-assisted phenomena is experimentally highly challenging as these experiments require the combination of very low temperatures and microwave radiation. Transport spectroscopy as described above has to be performed in a dilution refrigerator at temperatures of $\approx$100 mK. This complicates the application of externally generated microwave radiation over a wide frequency range as one is limited by losses in cables, heating effects and the space available in the refrigerator. The coupling of the radiation to the device under investigation has to be achieved with specially designed antennas. Utilizing the ac Josephson effect for tunable on-chip microwave sources represents a promising alternative approach to the realization of photon-assisted transport experiments circumventing the problems described. The most significant difference to usual experimental setups is the proximity of the microwave source to the structure of interest. So far, it is not clear whether and how the near-field properties of the source modifies photon-assisted transport.

Another fascinating aspect of future experiments on a double quantum dot with an embedded weak link is its relation to electrical quantum standards. Frequency locked pumping of electrons through multiple tunnel junctions has been demonstrated to serve as a current standard yielding a current $I = ef$ [37], or as a single electron counter [38]. In such devices, single electrons are pumped by appropriately raising and lowering

the tunnel barriers, i.e. gate voltages. Due to the probabilistic nature of tunneling, the accuracy of the pump decays rapidly for frequencies typically higher than 10–50 MHz as then some electrons will not tunnel each cycle. Furthermore, the metallic gates are effectively shunted at high frequencies disabling controlled turnstile operation. Thus, the attainable pump current through such a turnstile is only a few picoampere. It is an interesting question whether coherent tunneling through double dot systems at GHz frequencies could pump accordingly higher currents. A combination of a double quantum dot and one or several weak links enables us to investigate such pumping processes driven by the ac Josephson effect.

Acknowledgements—We would like to thank W. Zwerger, T. M. Klapwijk and M. Büttiker for stimulating discussions, and A. Kriele, S. Manus and W. Gödel for their continuous support. We also thank R. J. Warburton for a critical reading of the manuscript. The work was funded by the Volkswagen foundation under grant # I/68769 and the Deutsche Forschungsgemeinschaft (SFB 348).

References

[1] B. Irmer, R. H. Blick, F. Simmel, W. Gödel, H. Lorenz, and J. P. Kotthaus, Appl. Phys. Lett. **73**, 2051 (1998).
[2] B. J. van Wees, H. van Houten, C. W. J. Beenakker, J. G. Williamson, L. P. Kouwenhoven, D. van der Marel, and C. T. Foxon, Phys. Rev. Lett. **60**, 848 (1988); D. A. Wharam, T. J. Thornton, R. Newbury, M. Pepper, H. Ahmed, J. E. F. Frost, D. G. Hasko, D. C. Hasko, D. C. Peacock, D. A. Ritchie, and G. A. C. Jones, J. Phys. **C21**, L209 (1988).
[3] L. P. Kouwenhoven, C. M. Marcus, P. L. McEuen, S. Tarucha, R. M. Westervelt, and N. S. Wingreen, *Mesoscopic Electron Transport*, NATO ASI Series E, edited by H. Grabert, J. M. Martinis, and G. Schön (Kluwer, Dordrecht, 1997) and references therein.
[4] B. D. Josephson, Possible new effects in superconductive tunneling, Phys. Lett. **1**, 251 (1962); B. D. Josephson, The relativistic shift in the Mössbauer effect and coupled superconductors, Dissertation for the annual election of fellows, Trinity College, Cambridge, (1962).
[5] J. E. Zimmermann and A. H. Silver, Phys. Rev. **141**, 367 (1966).
[6] H. A. Notarys and J. E. Mercerau, J. Appl. Phys. **44**, 1821 (1973).
[7] P. W. Anderson and A. H. Dayem, Phys. Rev. Lett. **13**, 195 (1964).
[8] T. M. Klapwijk and J. E. Mooij, ASC **74**, 858 (1974).
[9] K. K. Likharev, Rev. Mod. Phys. **51**, 101 (1979).
[10] J. C. Swihart, J. Appl. Phys. **32**, 461 (1961).
[11] K. K. Likharev and B. T. Ulrich, *Josephson Junction Circuits and Applications* (Izd. Mosk. Universiteta, Moscow, 1978).
[12] T. M. Klapwijk and T. B. Veenstra, Phys. Lett. **A47**, 351 (1974).
[13] A. H. Dayem and J. J. Wiegand, Behavior of thin-film superconducting bridges in a microwave field, Phys. Rev. **155**, 419 (1967).
[14] R. Y. Chiao, M. J. Feldman, H. Ohta, and P. T. Parrish, Fabrication of small microbridges, Rev. Phys. Appl. **9**, 183 (1974).
[15] J. E. Mooij, C. A. Gorter, and J. E. Noordam, Rev. Phys. Appl. **9**, 173 (1974).
[16] M. Wendel, B. Irmer, J. Cortes, J. P. Kotthaus, A. Lorke, and E. Williams, Superlatt. Microstruct. **20**, 349 (1996).
[17] H. Lorenz, J. Lechner, and I. Eisele, Surf. Coat. Technol. **47**, 746 (1991); C. A. Davis, G. A. J. Amaratunga, and K. M. Knowles, Phys. Rev. Lett. **80**, 3280 (1998).
[18] NanoTooLS GmbH, Schillerstr. 6, 85101 Lenting, Germany (info@nano-tools.com).
[19] J. Hay, Applied Nano Metrics, Stormville, NY 12582, U.S.A.
[20] I. O. Kulik and A. N. Omelyanchuk, Sov. J. Low. Temp. Phys. **3**, 945 (1977).

[21] V. Ambegaokar and A. Baratoff, Phys. Rev. Lett. **10**, 86 (1963).
[22] BCS theory predicts a numerical factor of 3.52, whereas experiments on bulk Al give $3.37 \pm .1$; see, for example, *Handbook of Chemistry and Physics* (CRC Press, Boston, 1992) 72nd edition
[23] M. Tinkham, *Introduction to Superconductivity*, edited by Bayne Bredford and Michael Gardner (Robert E. Krieger Publishing Company, New York, 1996) 2nd edition, pp. 93–94.
[24] A. V. Zaitsev and D. V. Averin, Phys. Rev. Lett. **80**, 3602 (1998).
[25] A. Barone and G. Paterno, *Physics and Applications of the Josephson Effect* (John Wiley & Sons, New York, 1982).
[26] G. M. Daalmans, T. M. Klapwijk, and J. E. Mooij, Superconducting microbridges in Delft **ASC76**, 719 (1976).
[27] L. Y. Gorelik, N. I. Lundin, V. S. Shumeiko, R. I. Shekhter, and M. Johnson, Phys. Rev. Lett. **81**, 2538 (1998); D. Averin and A. Bardas, Phys. Rev. Lett. **75**, 1831 (1995).
[28] R. A. Wyss, C. C. Eugster, J. A. del Alamo, and Qing Hu, Appl. Phys. Lett. **63**, 1522 (1993); R. A. Wyss, C. C. Eugster, J. A. del Alamo, Qing Hu, M. J. Rooks, and M. R. Melloch, Appl. Phys. Lett. **66**, 1144 (1995).
[29] P. K. Tien and J. P. Gordon, Phys. Rev. **129**, 647 (1963).
[30] M. Büttiker and R. Landauer, Phys. Rev. Lett. **49**, 1739 (1982).
[31] L. P. Kouwenhoven, S. Jauhar, J. Orenstein, P. L. McEuen, Y. Nagamune, J. Motohisa, and H. Sakaki, Phys. Rev. Lett. **73**, 3443 (1994).
[32] R. H. Blick, R. J. Haug, D. W. van der Weide, K. von Klitzing, and K. Eberl, Appl. Phys. Lett. **67**, 3924 (1995).
[33] T. H. Oosterkamp, L. P. Kouwenhoven, A. E. A. Koolen, N. C. van der Vaart, and C. J. P. M. Harmans, Phys. Rev. Lett. **78**, 1536 (1997).
[34] T. H. Oosterkamp, T. Fujisawa, W. G. van der Wiel, K. Ishibashi, R. V. Hijman, S. Tarucha, and L. P. Kouwenhoven, subm. to Nature (1998).
[35] C. A. Stafford and N. S. Wingreen, Phys. Rev. Lett. **76**, 1916 (1996).
[36] R. H. Blick, D. W. van der Weide, R. J. Haug, and K. Eberl, Phys. Rev. Lett. **81**, 689 (1998).
[37] L. J. Geerligs, V. F. Anderegg, P. A. M. Holweg, J. E. Mooij, H. Pothier, D. Esteve, C. Urbina, and M. H. Devoret, Phys. Rev. Lett. **64**, 2691 (1990).
[38] M. W. Keller, J. M. Martinis, N. M. Zimmerman, and A. H. Steinbach, Appl. Phys. Lett. **69**, 1804 (1996).